N87-27213

RUPTURE TESTING FOR THE QUALITY CONTROL OF ELECTRODEPOSITED COPPER INTERCONNECTIONS IN HIGH-SPEED, HIGH-DENSITY CIRCUITS

Louis Zakraysek
General Electric Company
Syracuse, NY

Introduction

The performance requirements of copper-clad laminates and printed wiring boards are driven by advances in integrated circuit technology and by the resultant miniaturization of components. The trends in this technology have resulted in sophisticated multilayer versions of the basic laminate structure. Some examples of high density printed wiring multilayer boards (PWMLBs) are shown in Figure 1.

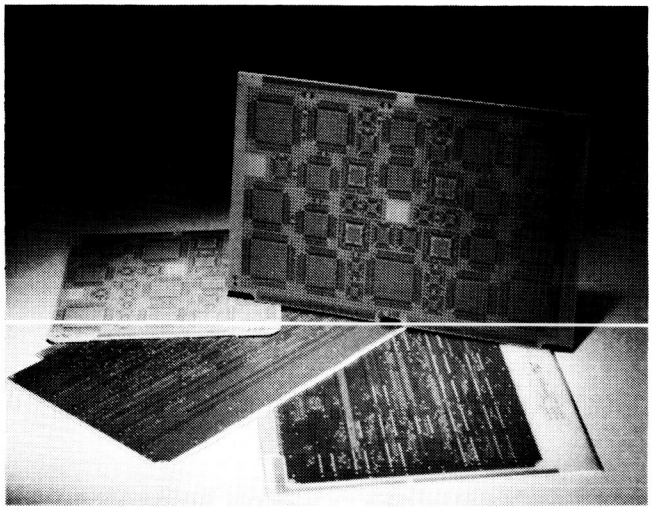

Figure 1. High-density printed wiring multilayer boards.

The most recent impetus for performance improvement stems from the desirability for the surface mounting of components, from the electrical and thermal constraints imposed by high density component assembly, and by high-speed circuit design. These advances make it imperative that we construct PWMLBs with predictable and consistent properties in order to meet performance needs.

Recent experience[1,2] in using advanced, thermally stabilized multilayer substrates for high density assemblies shows that they are susceptible to premature failure due to the microcracking of the interconnecting conductive traces, including both the inner layer foil and the plated-through-hole (PTH). In some cases, fracture is initiated by a thermal stress, and the microcrack propagates during thermal cycling. In other cases, failure occurs by a tensile over-stress or by creep-rupture. For either failure mechanism, the result is an open circuit condition and the loss of a completed, and usually expensive, PWMLB.

Shown in Figure 2 are the three usual locations where microcracking will occur, namely, at the PTH corner, in the PTH barrel, and at an inner layer. Examples of these fractures taken from PTH microstructures are shown in Figure 3. Fractures such as those shown here are caused by an excessive tensile stress during thermal shock, by creep-rupture due to a sustained thermal stress or by fatigue during thermal cycling. The fracture surfaces are typically those of brittle materials, i.e., little or no evidence of plastic deformation.

Whether or not fracture actually occurs in a given PWMLB appears to be dependent on three factors: (1) a Z-direction thermal stress of sufficient magnitude to initiate fracture, (2) design- or process-induced stress risers, and (3) the presence of electrolytic copper with low hot strength. To date, most of the attention with regard to microcracking has been given the first two. In this paper we describe a modified rupture pressure testing procedure by which the mechanical properties of copper conductors in PWMLBs can be quantified with respect to strength and ductility at elevated temperatures. Since this information is obtained before the copper is used in a PWMLB, it can be used to prevent the use of a grade of electrolytic copper that is susceptible to premature thermal stress failure. In addition to eliminating failure under some conditions, this approach provides some latitude with regard to the handling of the other two factors that are mentioned as contributors to microcracking.

Type of Interconnecting Material

A printed wiring board (PWB) is the primary method used in the electronics industry for the interconnection of circuits. A large share of the PWBs in use are produced by the fabrication of copper-clad laminates from which the copper is selectively removed by a photolithographic process to define a circuit interconnection pattern. Most of the copper used as conductor traces is supplied to laminators by a relatively small number of producers who make it in foil form by electrolytic deposition. The laminator then applies this foil to a dielectric substrate for subsequent sale to the PWB fabricator.

When the user of the laminates completes the fabrication of a multilayer printed wiring board, the circuit traces on each of the individual layers are interconnected by a plated-through-hole (PTH) process. Therefore, all of the conductors on a structure such as this are made of electrolytic copper, the surface and inner layers being done by an outside source, and the PTH deposition being done by an in-house plating operation. In this paper, either of these conductors will be referred to as Type E copper. The industry standard for Type E copper foil is IPC-CF-150 (Institute for Interconnecting and Packaging Electronic Circuits), and in this standard are documented the various classes of foil according to their mechanical-physical properties. The classes that are of most interest for our purpose, are Type E, Class 1; Type E, Class 3; and Type W, Class 7. They are, respectively: electrolytic, ordinary quality; electrolytic, high-temperature ductile; and rolled, annealed.

It should be noted that rolled foil (Type W, Class 7 in the above-mentioned standard) is also used on PWB laminates. For a number of reasons, its use is limited mostly to special applications such as

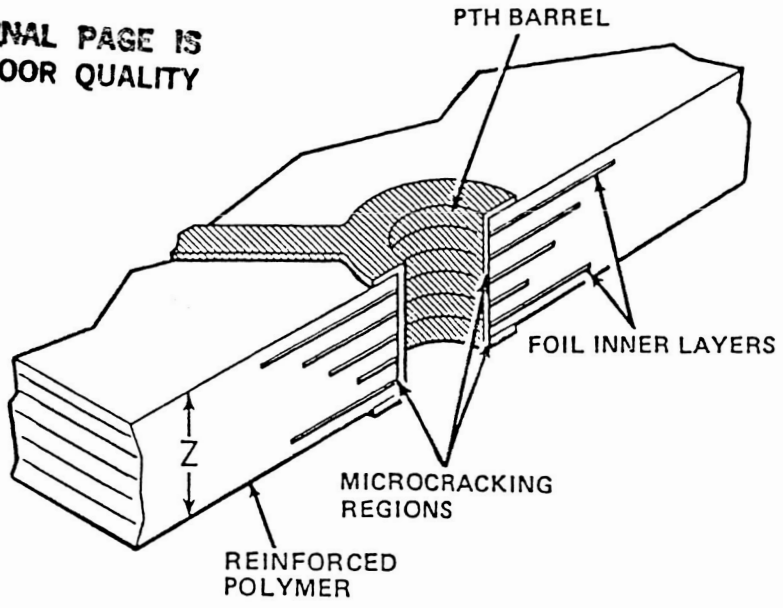

Figure 2. Section view of a PW multilayer board.

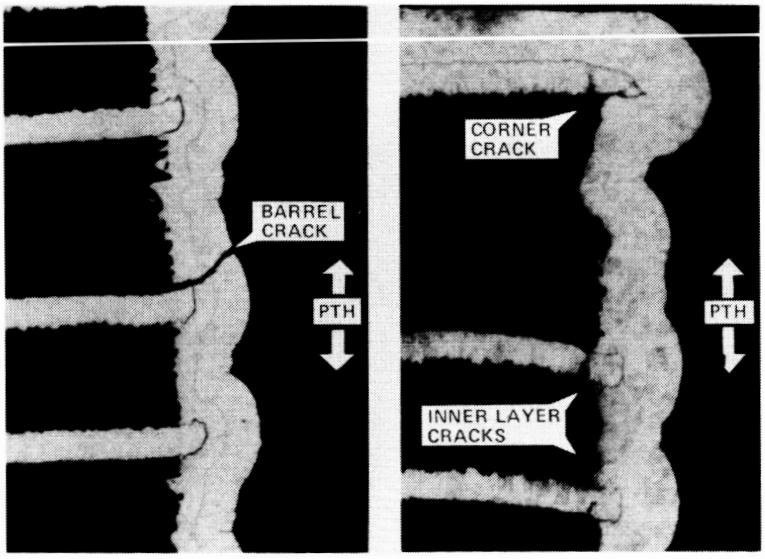

Figure 3. PWMLB plated-through-hole microstructures.

flexible circuits where consistently high ductility is essential. Obviously, Type W copper is not viable for PTH use, so in the case of multilayer circuits where rolled foil is used for inner layers, the PTH interconnections are still electrolytically deposited (Type E). At any rate, since Type W, Class 7 is a product of a totally different process, it makes a very good baseline for comparing metallurgical characteristics with the Type E classes.

Without too much difficulty, foil samples can also be obtained from an in-house PTH operation, in which case any of the procedures, standards, etc. developed for the commercial foils will apply to them so long as care is taken to avoid the introduction of plating artifacts that might influence the properties of the samples. This allows any of the controls that are used for commercial foil to be used for PTH copper, with the objective of gaining in-house PTH process control by this means.

The Control of Microcracking in Type E Copper

As had been mentioned earlier, the microcracking of copper interconnections has been found[3] to occur in high density PWMLBs regardless of the technology that is used in board fabrication. That is, cracks occur in inner layers or in the PTH barrel when any of the most advanced types of PWMLB structures are thermally stressed. There is evidence[4] that the stresses that cause microcracking are generated by the Z-direction (through-the-thickness) thermal expansion of the substrate material. The problem is that, when this thermal stress is applied to a Type E, Class 1 grade of copper, fracture without deformation will occur at low stress levels. The cracking phenomenon is thought[5] to arise from the combination of a thermal stress together with a copper plate in which grain boundary strength has been degraded. Further, this degradation is thought to be due to the presence of co-deposited impurities (esp. organics) that cause easy grain boundary separation at elevated temperatures. Some evidence of the lack of hot ductility in Class 1 copper can be seen from a comparison of the fracture surfaces of the foil samples in the scanning electron micrographs shown in Figure 4. In this case, the Type W, Class 7 material shows extensive shear and elongation in both the RT and the elevated temperature fractures. Although not as pronounced, the Type E, Class 3 material also exhibits a shear component at either test temperature. For Type E, Class 1 foil, the RT fracture shows slight deformation while the 550°F fracture is brittle.

When the ductile Class 3 and the brittle Class 1 foils are examined by metallographic sectioning, a similar comparison can be made, as is shown in Figure 5. The microstructure near the fracture exibits considerable elongation in the ductile foil and no elongation in the brittle material. This is an important distinction between the Class 1 and Class 3 types of material, and it is this difference that we must be able to detect if quality control is to be effective.

This also implies that Type E, Class 1 copper foil (or its PTH copper equivalent deposit) should not be used in PWMLBs where a Z-direction thermal stress is likely to be applied. When this condition exists, Type E, Class 3 (or its PTH equivalent) should be used. For foil, its quality can be controlled by proper procurement policy, and for a

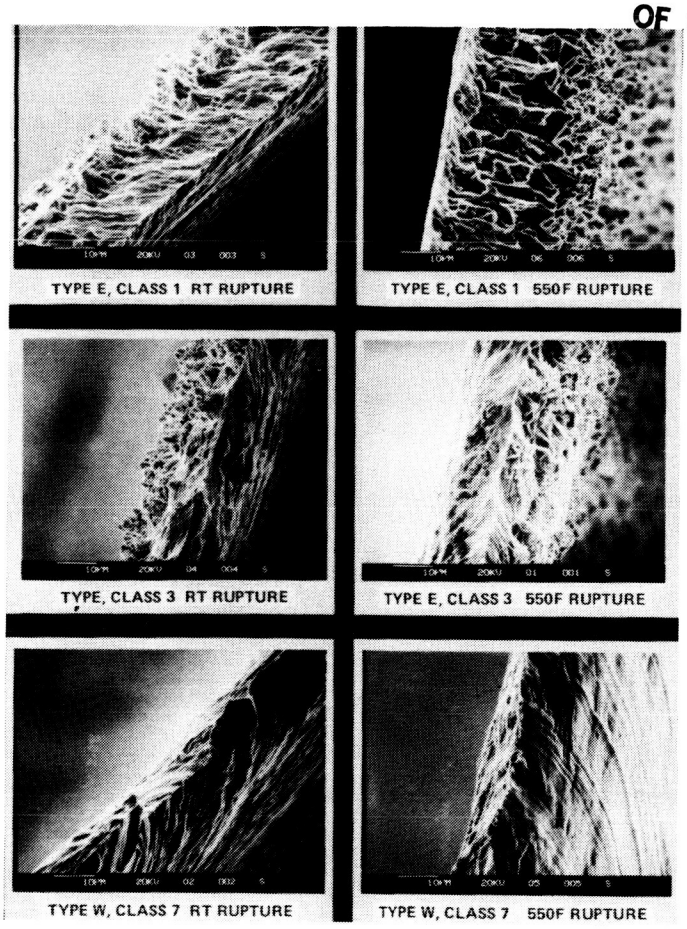

Figure 4. Copper foil rupture fracture surfaces.

plated-through-hole, quality can be maintained through the use of process controls that prevent the contamination of copper deposits, e.g., in a PWMLB PTH operation. One effective procedure for plating bath analysis resulted from the recent practical development of cyclic voltametry[6], and this technique is now available to the industry. However, along with a capability for monitoring the condition of the plating solution, there is a need for determining and monitoring the elevated temperature mechanical properties of the resultant deposit. Control over these properties can provide control of the microcracking phenomenon. In this paper, we suggest a test method for this purpose.

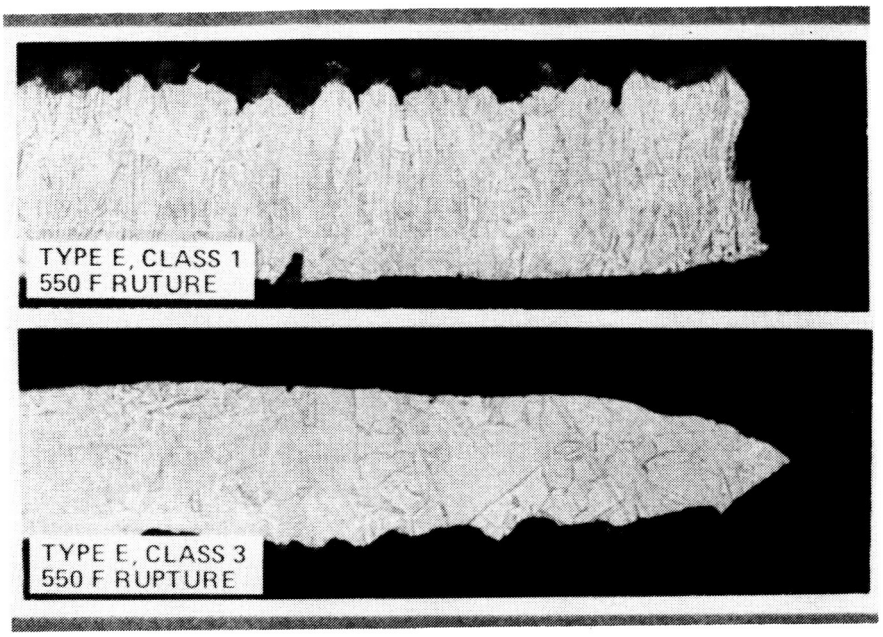

Figure 5. 550°F rupture microsections. Top: type E, class 1, brittle fracture; bottom: type E, class 3, ductile fracture 800X0.

Hot Rupture Testing

A procedure for the bulge testing of samples of electrolytic foil is described in some detail by Prater[7,8] and Read as a result of their pioneering work in this area of technology. This contribution was followed by Lamb and co-workers[9] who determined the mechanical properties, including rupture pressure, of Type E copper as deposited from the commonly available copper plating solutions. More broadly, the Mullen hydraulic bulge test, or some adaptation of it, is widely used[10-11] for determining the stress-strain properties of sheet metals for the control of forming characteristics.

Rupture testing is uncomplicated, with no special requirement for sample preparation when testing thin sheets or foils. However, as our previous discussion indicates, determining the important properties for Type E copper in PWMLBs depends on having an elevated temperature testing capability that is not available on hydraulic machines. To overcome this

limit, a new method was established around the use of pneumatic pressure. Figure 6 shows, in block form, our procedure for determining mechanical properties by rupture testing. By this process, the effect of either a dynamic or a static pressure can be determined at any temperature up to 550°F which is the highest processing, test or use temperature encountered by most PWMLBs.

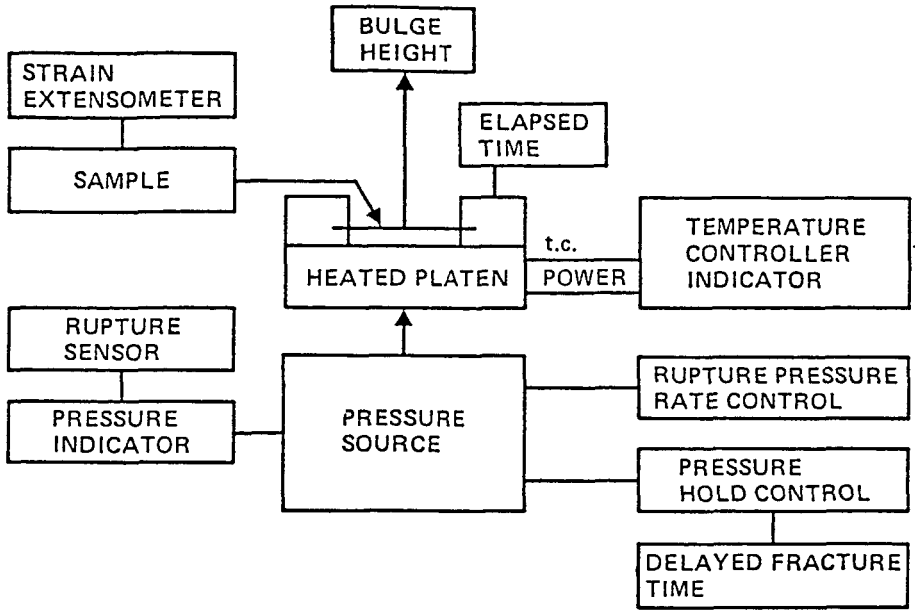

Figure 6. Procedure for the hot rupture testing of foil.

Dynamic Rupture Test. In this test, a constant loading rate of 1 psig/sec is applied to the test piece while it is held at a constant test temperature. Measurements are made for bulge height at 10 psig intervals. The bulge height at rupture and the rupture pressure for each test temperature are recorded. Since this test yields data points for pressure, bulge height and temperature, any combination of these variables can be used for an evaluation of material properties. However, for quality control purposes, a valid comparison between foil types is most easily obtained by a plot of rupture pressure versus test temperature. From these data, a measure of mechanical strength and ductility can be obtained.

When a pressure is applied to the foil, the foil deforms under balanced biaxial tension, and this deformation continues until fracture occurs. From the measured values for rupture pressure and bulge height, from the geometry of an axisymmetrical bulge [1], and from membrane stress and strain relationships [2] for thin walled pressure vessels, we can make comparisons with values obtained from a uniaxial tensile test, as follows:

$$R = \frac{r^2 + h^2}{2h} \qquad [1]$$

where R is the radius of curvature, r is the radius of the aperture, and h is the height of the bulge. Then, we can obtain tensile strength from:

$$TS = \frac{PR}{2t} \qquad [2]$$

where TS is the nominal tensile strength, P is the rupture pressure, R is the radius of curvature and t is the original thickness. These mathematical relationships are more fully developed in the literature[12-15] where it is shown that obtaining true stress, true strain, nominal strain, ductility, and elongation values from bulge rupture tests can be achieved by taking into account the basic differences between the tensile test and the rupture test. However, this degree of detail is probably not necessary for effective use of the rupture test for quality control purposes.

Creep-Rupture Test. This procedure differs from the dynamic approach only in that a pre-set, constant pressure is applied and an up-counting timer is used for the measurement of the delayed-fracture time at constant pressure. Otherwise, the test equipment is identical. In either case, the assembly is designed such that tests can be made at any temperature between RT and 550°F, and at any pressure up to 80 psig. To allow the testing to be done on the same pressure scale, the cover plate aperture is variable for accommodating 1/2 ounce or 1 ounce foils.

Creep-rupture properties are obtained by the application of a constant pressure at constant temperature. Measurement is made for the time-to-rupture at each test pressure, and a plot of rupture pressure versus time at any test temperature will distinguish between the different types of copper. Typically, the nearer to the rupture pressure that the test pressure is set, and the higher the test temperature, the shorter is the time to fracture. Also, there is a distinctive difference in the delayed fracture characteristics of the various types and classes of foil and this allows their segregation according to rupture quality.

Mechanical Testing of Foil. Shown in Figure 7 is the mechanical set-up for the testing of 1/2 ounce and 1 ounce copper foil. For this test, sample pieces are cut into 4 X 4 inch squares. Nine test pieces are needed per lot, with three being used at each of three test temperatures (RT, 350, and 550°F) for a measure of dynamic rupture properties. For determining delayed-fracture characteristics, at least six test pieces are needed per lot, with three being used at each of two test pressures and one test temperature (350°F). As is true of the dynamic version, this test can be conducted over a much broader set of pressure, temperature or time test conditions if so desired.

From its flat initial condition, the resultant test piece takes on a hemispherical shape due to the applied pressure. The radius of curvature and the height of the bulge vary, of course, from sample to sample as can be seen from the collection of tested pieces shown in Figure 8.

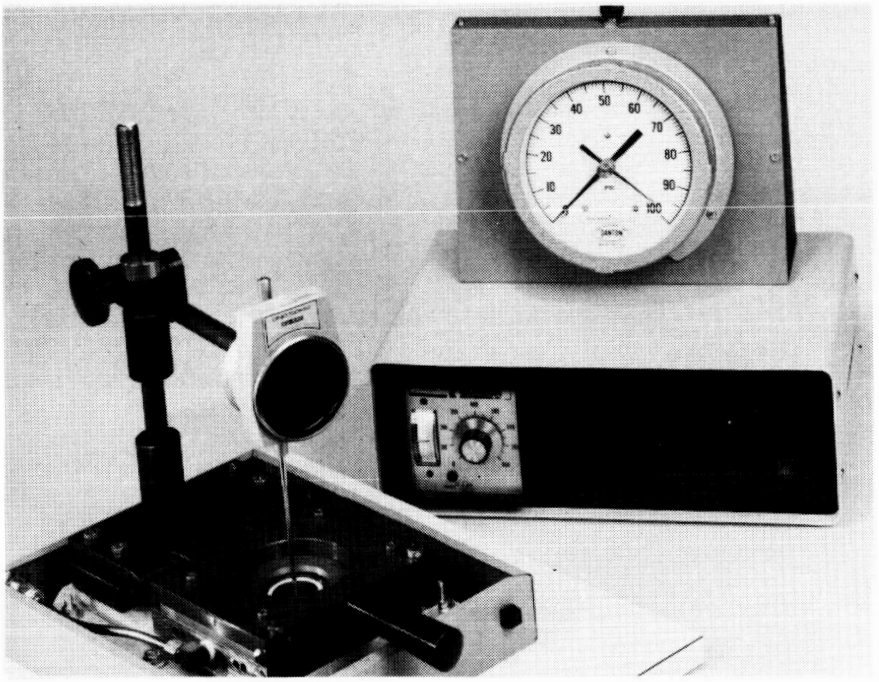

Figure 7. Foil rupture testing machine.

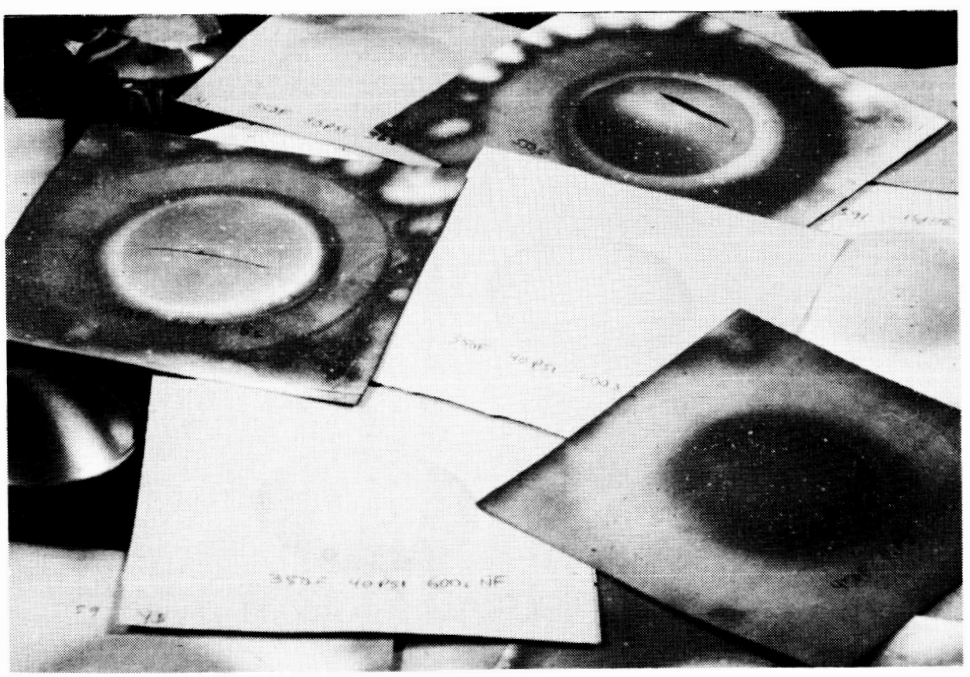

Figure 8. Typical rupture test samples: 10 cm square, aperture 2.

Setting Quality Control Standards - Dynamic Rupture

Numerous tests were made on 1/2 ounce and 1 ounce Type E and Type W copper foils. Commercial material representing foil production from the major foil suppliers was used to establish plots of rupture pressure versus test temperature for each type of foil at the two thickness levels. In an iterative process, the initial plots were used to classify larger numbers of foil and these results were then used further to refine the standards. Following this procedure, standard plots were developed and now exist for Type E, Class 1; Type E, Class 3; and Type W, Class 7 foils.

Figure 9 shows the effect of test temperature on the rupture pressure of 1 ounce Type E, Class 1 copper foil. Under these test conditions, the average rupture pressure at the solder-float temperature (550°F) is about 40% of that at room temperature. Of even more concern are the lowest rupture values, which have ranged down to 6 psig when the foil is stressed at the highest test temperature.

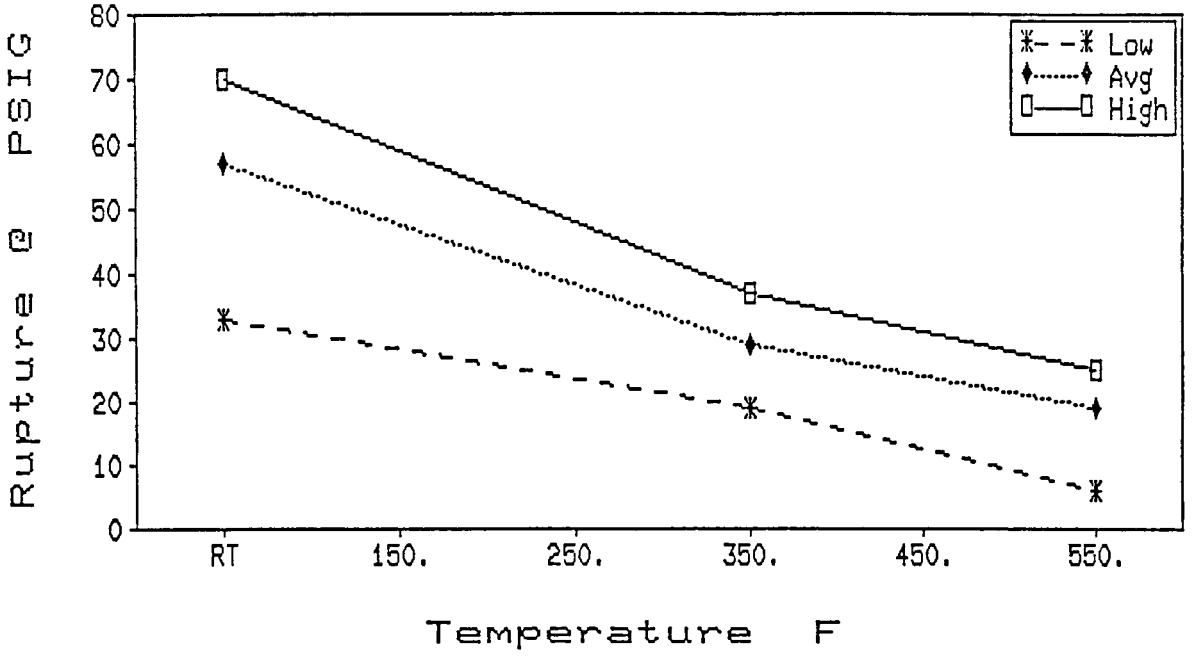

Figure 9. P versus T standard, type E, class 1, copper (1 oz).

This set of curves then are those that represent copper foil that is of Type E, Class 1 quality.

Figure 10 shows the effect of test temperature on the rupture pressure of 1 ounce Type E, Class 3 copper foil, and Figure 11 shows the results for Type W, Class 7 foil. These results show that the average rupture pressure at 550°F is over 60% of that at RT for these foils. Better yet, they maintain rupture strengths of over 35 psig at solder float temperatures, a significant improvement over Class 1 foil. The other observation worth mentioning is that the Class 1 foil properties extend

into the Class 3 and Class 7 property range at RT, so the elevated temperature tests will provide a more positive indication of the correct foil classification. In other words, RT testing is probably not sufficient for proper foil characterization.

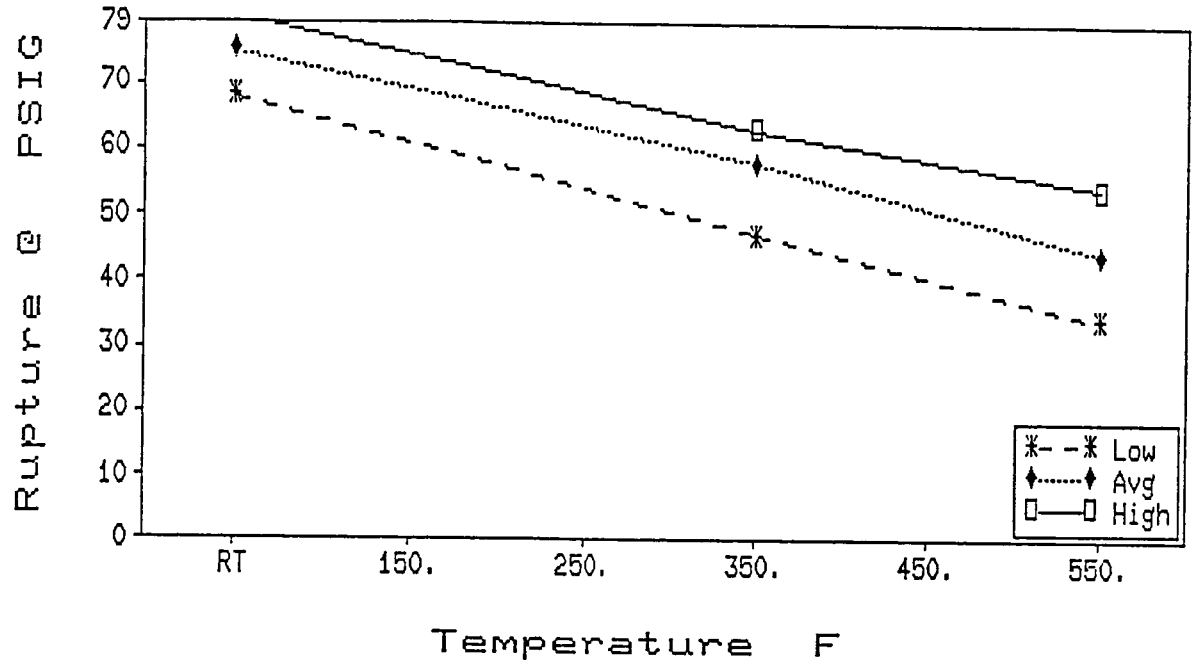

Figure 10. P versus T standard, type E, class 3 copper (1 oz).

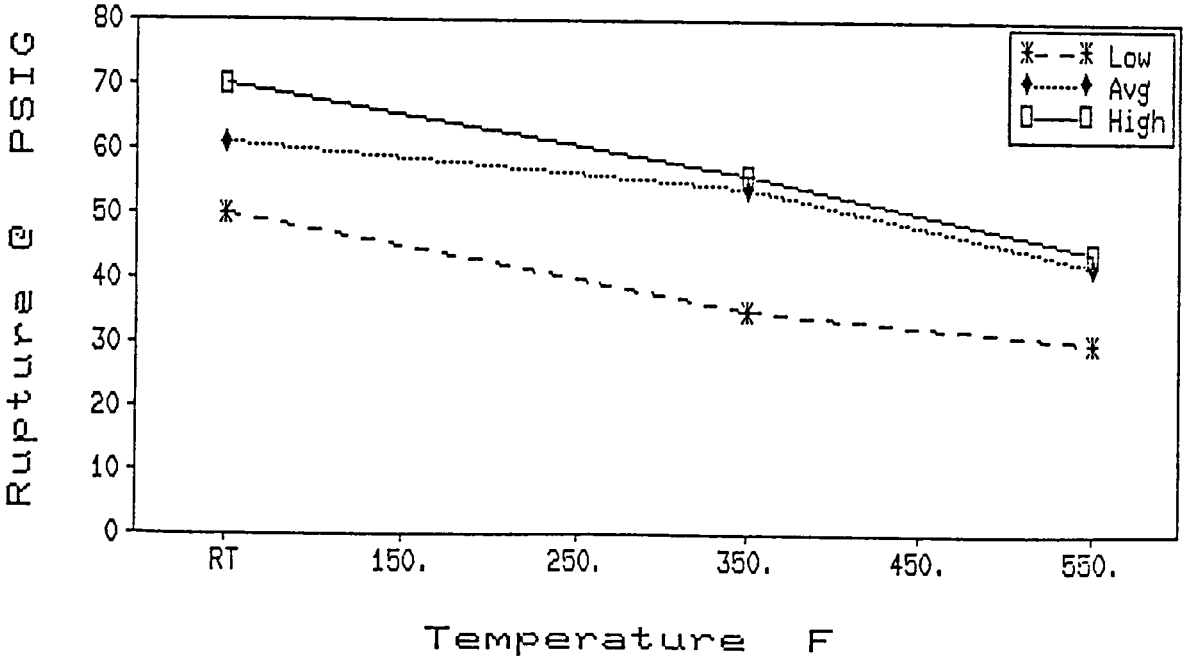

Figure 11. P versus T standard, type W, class 7 copper (1 oz).

Foil Characterization. Other than for material characteristics, rupture test results are influenced most by strain rate, by creep and by sample thickness. Shown in Figure 12 is the effect of strain rate for rolled, annealed foil. Figure 13 shows the effect of thickness for the various types of foils when a room temperature test is done at a strain rate of 1 psig/second.

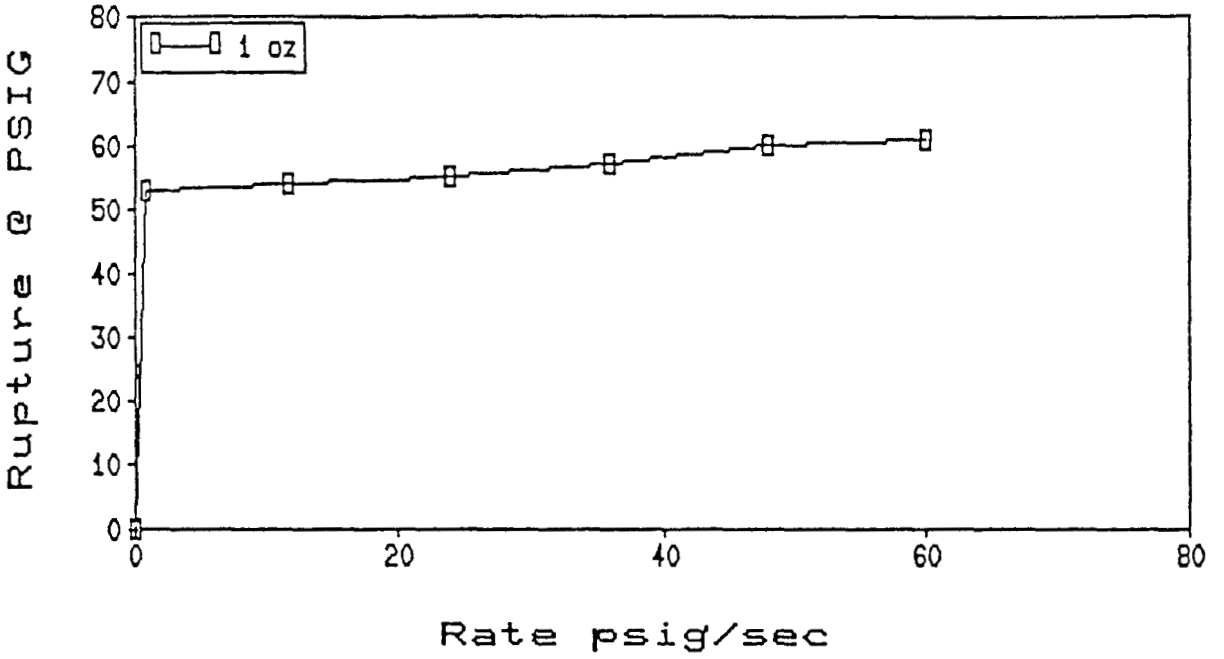

Figure 12. Effect of strain rate, type W, class 7 foil.

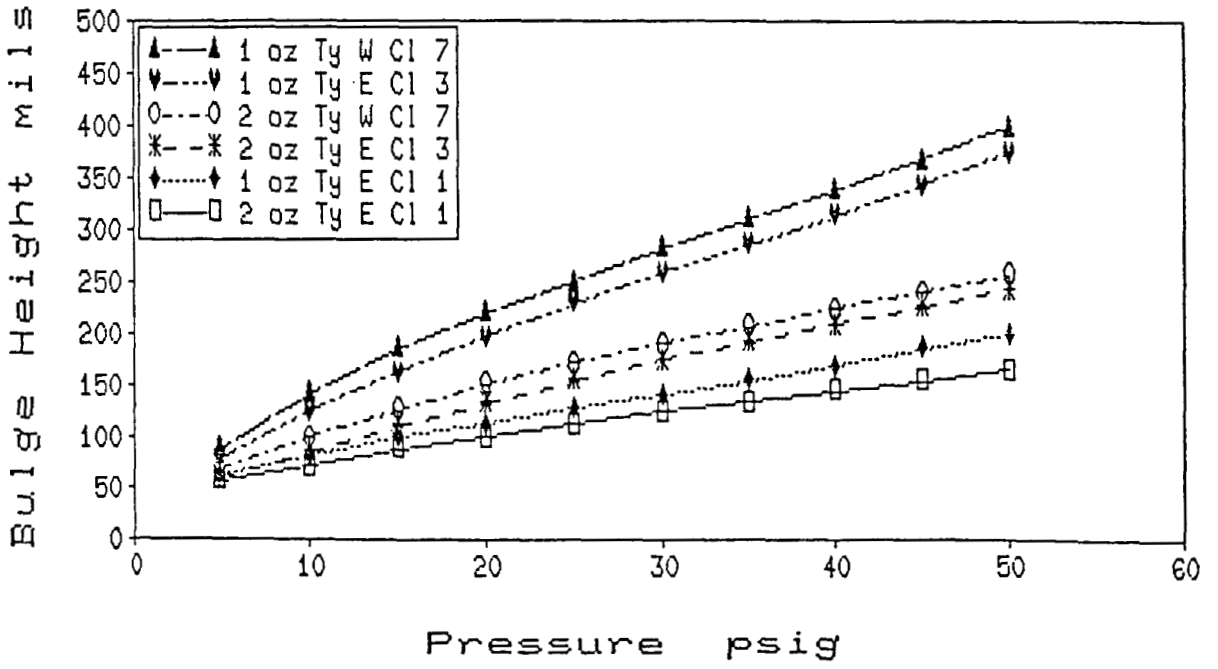

Figure 13. Effect of foil thickness, RT test, A2 Ty E and Ty W foils.

The standards that have been established for these three foils can now be used for the classification of foils from new lots of material, and this grading can be done before the new foil is laminated or used in PWMLB fabrication. The rupture properties for several different types and classes of foil are shown in Figure 14 where rupture pressure is plotted against the test temperature. These rupture-strength data were taken for 1 ounce foil that was obtained from commercial suppliers of electrolytic and rolled copper foil. As expected, when the different types and classes of foils are categorized by their comparison against the set of standard plots, each falls into the classifications which had been developed earlier.

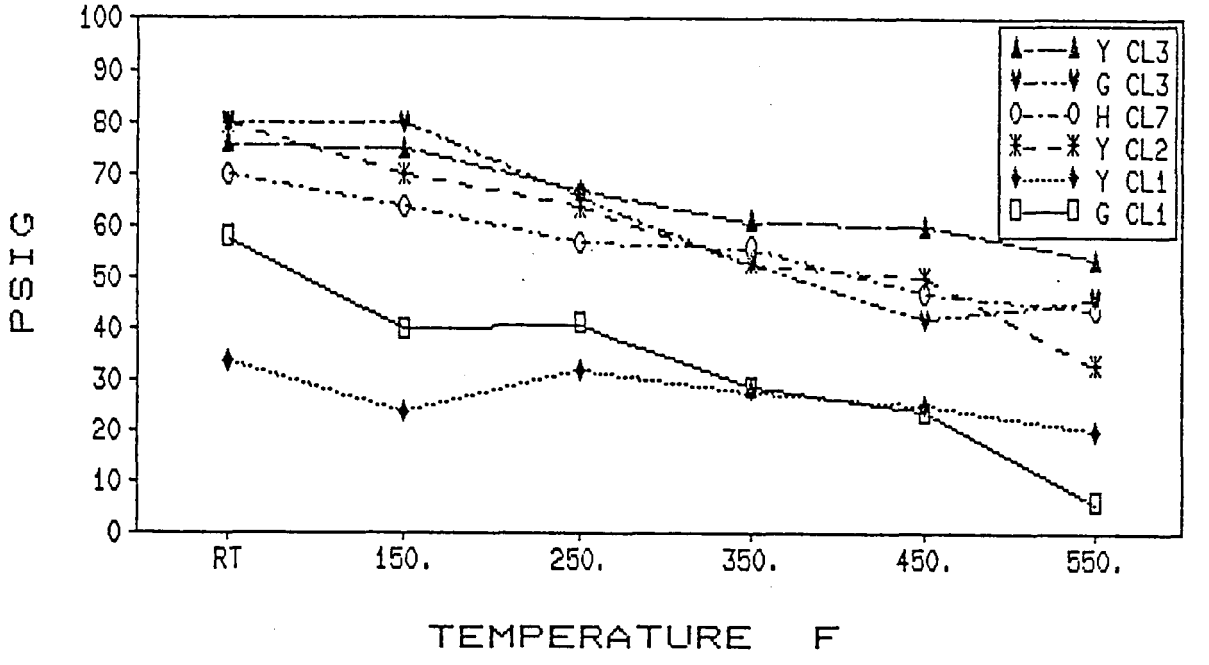

Figure 14. Rupture pressure versus temperature, Yates, Gould, and Hitachi **foils (1 oz).**

PTH Copper Characterization. As part of the classification process, foil samples from in-house PTH operations at several PWMLB facilities were made and tested. These samples represented copper deposits from the common plating solutions, including, sulfate, pyrophosphate and cyanide. When used in conjunction with the standards for the commercial foils, the PTH copper can be graded as being the equivalent of either the Class 1 or the Class 3 foil. In this way, PTH samples can be used to monitor the condition of the PWMLB plating process, i.e., through a determination of the mechanical properties at different times during the life of the plating bath.

As opposed to commercial foil, samples for the testing of PTH deposits must be obtained from the plating solution that is of interest. The objective is to make foil samples that can be used for the purpose of

determining the PTH equivalent of foil properties. This will enable us to use the same standards for PTH deposits as were used for commercial foil. Shown in Figure 15 is the panel-loading end of an automated PWMLB plating operation. To make foil test pieces, a polished stainless-steel panel is loaded in the rack in preparation for copper plating. The panel will pass through this plating line where it will be coated with either 1/2 ounce or 1 ounce of copper. Although plating conditions for a large, flat panel are not exactly like those in the local region of a PTH, the resultant deposit should be somewhat representative of the copper that would be deposited on a PWMLB. At the very least, foil made in this way provides a means for tracking the condition of a plating bath through the use of mechanical tests on the deposit, an approach that is commonly used for making tensile tests on plated deposits. Figure 16 shows how the plated copper is taken off the panel for testing. Once in foil form, the sample sheet can be sheared into 4 X 4 inch test pieces, to be tested for rupture strength in the same way that was previously described for the commercial foils.

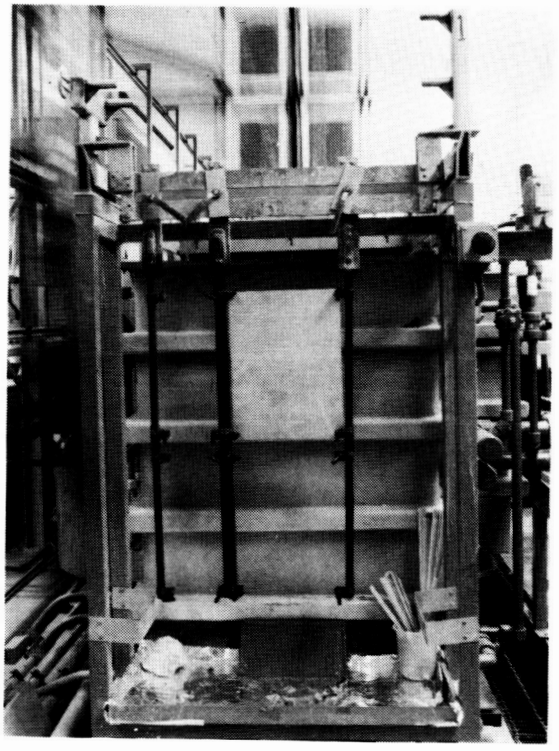

Figure 15. PTH foil panel.

Figure 16. PTH foil sample.

In this manner, test pieces were made from a PWMLB production plating line that uses acid copper sulfate plating chemicals. The initial bath

make-up, with regard to composition, additives, etc. was done according to the supplier's recommendations. A series of PTH foils were taken from this plating operation over a period of eight months, and the foil was tested for rupture properties by using the procedure described earlier. Shown in Figure 17 are the results of these tests.

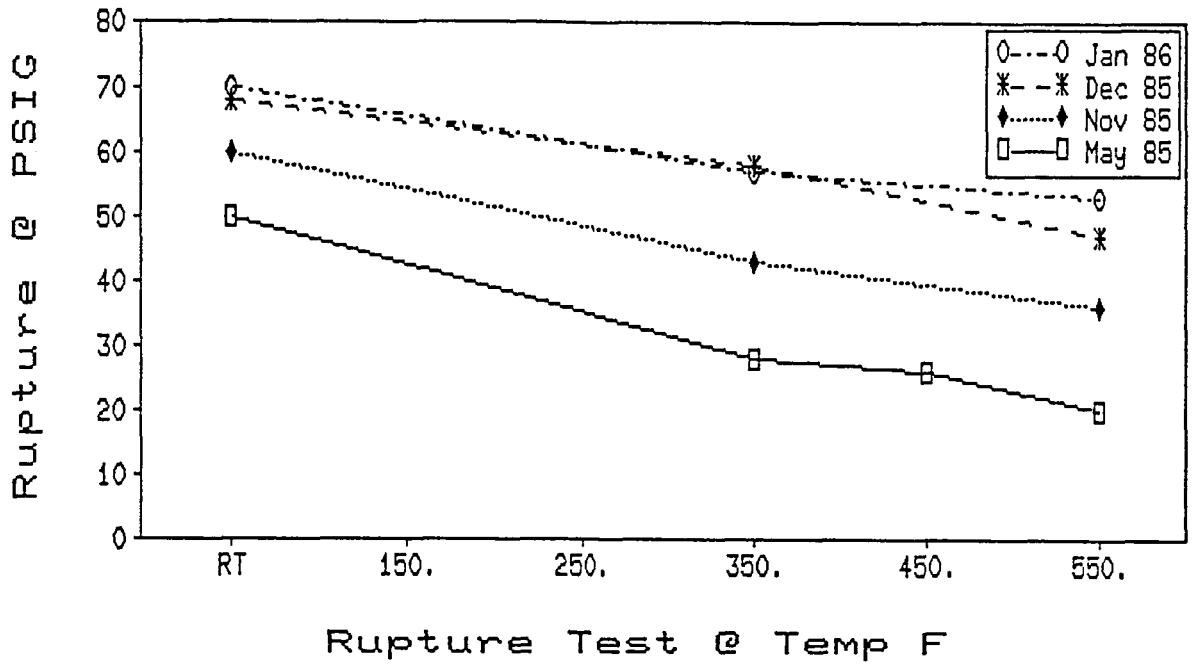

Figure 17. P versus T PTH Cu, acid copper (1 oz).

The easiest way to examine and to interpret these data is to overlay onto this set of curves the standard plots for Class 1 and Class 3 foil. When this is done, it can be seen that the May 85 PTH foil is in the average Class 1 category. The November 1985 PTH foil is just above Class 1 and into the lower level of the Class 3 quality range. The December 1985 and the January 1986 PTH foil materials are both well into the Class 3 quality range.

We mentioned that the plating bath represented by these foil samples is an acid copper sulfate solution. It should also be mentioned that the bath had been set up, in May 1985, to the supplier's recommendations. The PWMLB product from this plating line, at that time, exhibited PTH corner cracks in 50% of the boards. By November 1985, the plating bath was operating with modified quantities of additives, especially organic brighteners. This change is reflected in the improved rupture properties of the test pieces as well as in the total elimination of PTH corner cracks.

Quality Control by Creep-Rupture Testing

When a foil test piece is held at constant pressure and constant temperature, rupture occurs due to creep. A measure of time-to-fracture provides an indication of the creep-rupture resistance of the material

under test, and this characteristic varies according to the type of foil that is being tested. Using the static pressure test method, an evaluation was made of 15 lots of 1/2 ounce commercial foil. Shown in Figure 18 are the results as compiled for 10 lots of Type E, Class 1 foil.

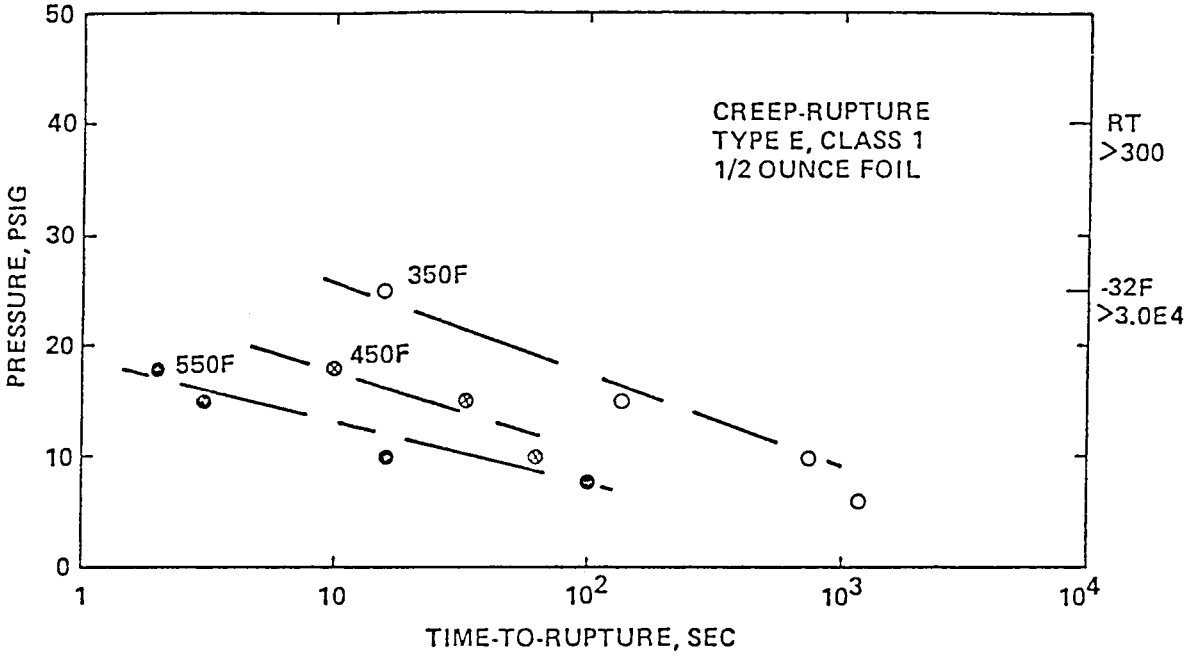

Figure 18. Effect of temperature on time-to-rupture at constant pressure, type E, class 1 foil; 1/2 oz.

These test results show that the time-to-rupture increases with decreasing pressure and that the creep-rupture pressure decreases with increasing temperature. More importantly, for Class 1 foil, rupture will occur in less than 10 seconds at pressure levels of from 12 to 25 psig when the foil is stressed at temperatures above 350°F. This implies that Type E, Class 1 inner layer or PTH interconnections could be damaged during solder-float testing where the requirement is for a 10 second exposure at 550°F. Also, thermal cycling, soldering or solder repair could cause fracture with some very moderate Z-direction stresses.

Static rupture tests were made on material from 5 lots of 1/2 ounce Type E, Class 3 foil. The results are shown in Figure 19 where it can be seen that the same trends are present with the Class 3 material as were noted with the Class 1 foil. An important difference is that the Class 3 foil has much better creep-rupture strength at any test temperature, e.g., relatively high pressures are needed in order to cause fracture in times under 10 seconds. This difference in delayed-fracture characteristics makes it possible to distinguish a quality difference between the two classes of foil through the use of the static rupture test method.

Another phenomenon which is peculiar to Type E, Class 3 material is evident upon examination of the 550°F test results. Since early creep-rupture does not occur, the foil is annealed during the test cycle. This improves the rupture properties of the foil, as would an anneal before the rupture test. This does not happen with Class 1 foil during the 550°F test.

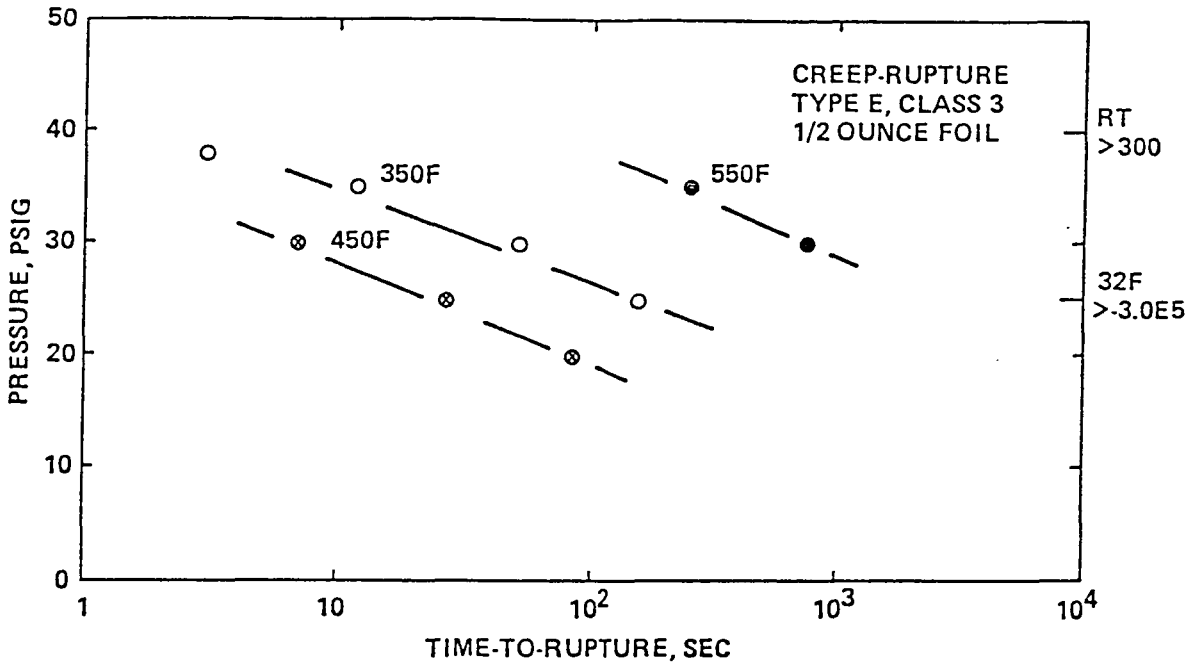

Figure 19. Effect of temperature on time-to-rupture at constant pressure, type E, class 3 foil; 1/2 oz.

Summary and Conclusions

PWMLB structures for high-speed, high-density circuits are prone to failure due to the microcracking of electrolytic copper interconnections. The failure can occur in the foil that makes up the inner layer traces or in the PTH deposit that forms the layer-to-layer interconnections.

In this paper, we show that there are some distinctive differences in the quality of Type E copper and that these differences can be detected before its use in a PWMLB. We suggest that the strength of some Type E copper can be very low when the material is hot and that it is the use of this poor quality material in a PWMLB that results in PTH and inner-layer microcracking.

Since the PWMLB failures in question are induced by a thermal stress, and since the poorer grades of Type E materials used in these structures are susceptible to premature failure under thermal stress, we propose the use of elevated temperature rupture and creep-rupture testing as a means for screening copper foil (or its PTH equivalent) in order to eliminate the problem of Type E copper microcracking in advanced PWMLBs.

References

1. R.A. Mogle and D.J. Sober, "Kevlar Epoxy for Chip Carrier MLBs", SI-928, NORTHCON '83, Portland, OR, May 11, 1983.

2. P. Hemler, et.al., "Hermetic Chip Carrier Compatible Printed Wiring Board", AFWAL-TR-85-4082, Final Report, July 1985, Contract No. F33615-82-C-5047, AFWAL/MLPO, WPAFB OH 45433.

3. G. Beene, et.al., "Manufacturing Technology for High Reliability Packaging Using Hermetic Chip Carriers (HCCs) on Compatible Printed Wiring Boards", Fifth Interim Report, June 1985, AFWAL Contract No. F33615-82-C-5071, AFWAL/MLTE, WPAFB OH 45433.

4. R.F. Clark, "Thermal-Mechanical Stress Analysis of Multilayer Printed Wiring Boards", GE Technical Information Series, R83ELS018, Nov. 1983.

5. R.F. Clark, H. Ladwig, and L. Zakraysek, "Microcracking in Electrolytic Copper", Printed Circuit World Convention III, IPC, May 1984.

6. D. Tench and C. Ogden, "Manufacturing Technology for PWB Electrodeposition Processes", AFWAL Contract No. F33615-81-C-5108, AFML, WPAFB, OH 45433, 1981.

7. T.A. Prater and H.J. Read, "The Strength and Ductility of Electrodeposited Metals, Part I", Plating, December 1949, p. 1221.

8. T.A. Prater and H.J. Read, "The Strength and Ductility of Electrodeposited Metals, Part II", Plating, Aug. 1950, p. 830.

9. V.A. Lamb, C.E. Johnson and D.R. Valentine, "Physical and Mechanical Properties of Electrodeposited Copper", J. Electrochemical Soc., Oct 1970, p. 341C.

10. F. Gologranc, "Automatic Determination of Stress-Strain Curves by Continuous Hydraulic Bulge Test", J. Mech. Eng., Strojniski Vestnik, Vol 26, No. 7-8, Ljubljana, July-Aug 1980.

11. R.F. Young, J.E. Bird and J.L. Duncan, "An Automated Hydraulic Bulge Tester", J. Applied Metalworking, ISSN 0162-9700/81/0701-0011, Vol 2, No. 1-11, American Society for Metals 1981.

12. H.M. Shang and T.C. Hsu, "Deformation and Curvatures in Sheet-Metal in the Bulge Test", J. Eng. for Industry, Aug. 1979, Vol 101, p. 341.

13. A.J. Ranta-Eskola, "Use of the Hydraulic Bulge Test in Biaxial Tensile Testing", Int. J. Mech. Sci., Vol 21, pp. 457-465, 1979.

14. A.S. Wifi, "Finite Element Correction Matrices in the Hydrostatic Bulging of a Circular Sheet", Int. J. Mech. Sci., Vol 24, No. 7, pp. 393-406, 1982.

15. M.F. Llahi, A. Parmar and P.B. Mellor, "Hydrostatic Bulging of a Circular Aluminium Diaphragm", Int. J. Mech. Sci., Vol 23, No. 4, pp. 221-227, 1981.

HETERODYNE HOLOGRAPHIC INTERFEROMETRY: HIGH-RESOLUTION RANGING AND DISPLACEMENT MEASUREMENT

James W. Wagner
The Johns Hopkins University
Center for Nondestructive Evaluation
Baltimore, Maryland

Heterodyne holographic interferometry (HHI) provides a means to map out-of-plane displacements and surface contours in full field with an out-of-plane resolution on the order of Angstroms. To gain an understanding of how this is done, three types of holographic interferometry will be considered - classical (homodyne) interferometry, quasi-heterodyne interferometry, and finally heterodyne interferometry. Note that each successive type represents an improvement, not only in resolution, but also in the dynamic range of the measurement.

Holographic Interferometry

Noncontact measurement of out-of-plane displacements over a range from:

- 125nm - 25um (homodyne)
- 1.25nm - 25um (quasi-heterodyne)
- 0.125nm - 25um (heterodyne)

Relatively few applications of HI, Q-HHI, or HHI in electronics packaging or assembly are documented in the open literature. However, Q-HHI and HHI are relatively new techniques whose full potentials have yet to be realized.

Applications in Electronics

(documented)

- Thermal-Mechanical Strain Analysis of Plated Through Holes in Multilayer Printed Circuit Boards
- Stress Analysis of Surface Mount Solder Connections
- Leak Detection and Measurement

This list of potential applications comes from a greater familiarity with holographic measurement technology than with electronic packaging and assembly. Note that since these techniques actually measure optical path length differences, they could be applied to measure nonuniformities in the composition or stress distribution of optically transparent materials (including silicon in the infrared).

Other Applications

- Warp and Flatness Measurements
- Vibration Analysis
- Uniformity of Properties of Materials for Integrated Optics
- Full Field Ultrasonic Detection for Debond and Composite Delamination

Classical homodyne holographic recordings are made using a high-resolution photographic emulsion exposed to the interference of a modulated object beam with a reference optical beam. The fine interference pattern which is recorded may be used as a complex diffraction grating to reconstruct the object wavefront by illumination of the hologram with the reference beam. Such holographic plates may be doubly exposed so that a single reconstructing reference beam will reconstruct two object wavefronts. Differences between the two objects will then result in interference fringes superimposed on the viewed image. Object differences may be imposed by stresses applied between exposures. Alternatively, one may use optical "tricks" to create an effective surface displacement proportional to the contour or the surface.

Homodyne Construction

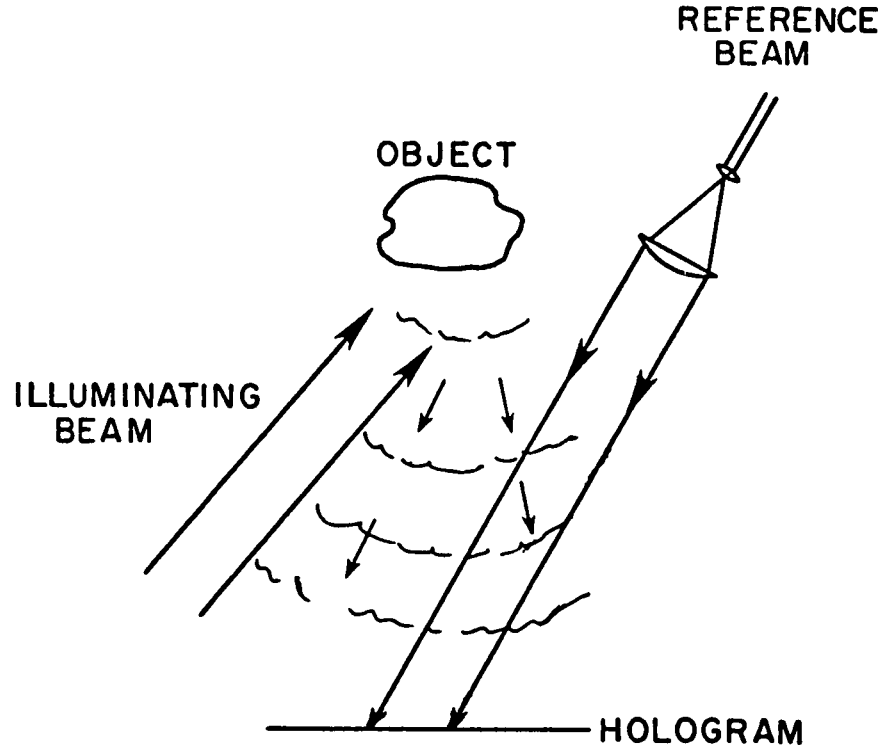

One "trick" for obtaining contour interferograms is to place the object to be contoured in a chamber filled with a fluid of known refractive index. Viewing the object through an optically flat window, an initial holographic recording is made. Prior to the second exposure, the fluid in the chamber is changed to one with a different refractive index. Upon reconstruction, the holographic interference pattern provides a contour map of the object surface.

In practice, we have used air as the refractive fluid in the test chamber. Its index is easily changed simply by changing the pressure within the chamber.

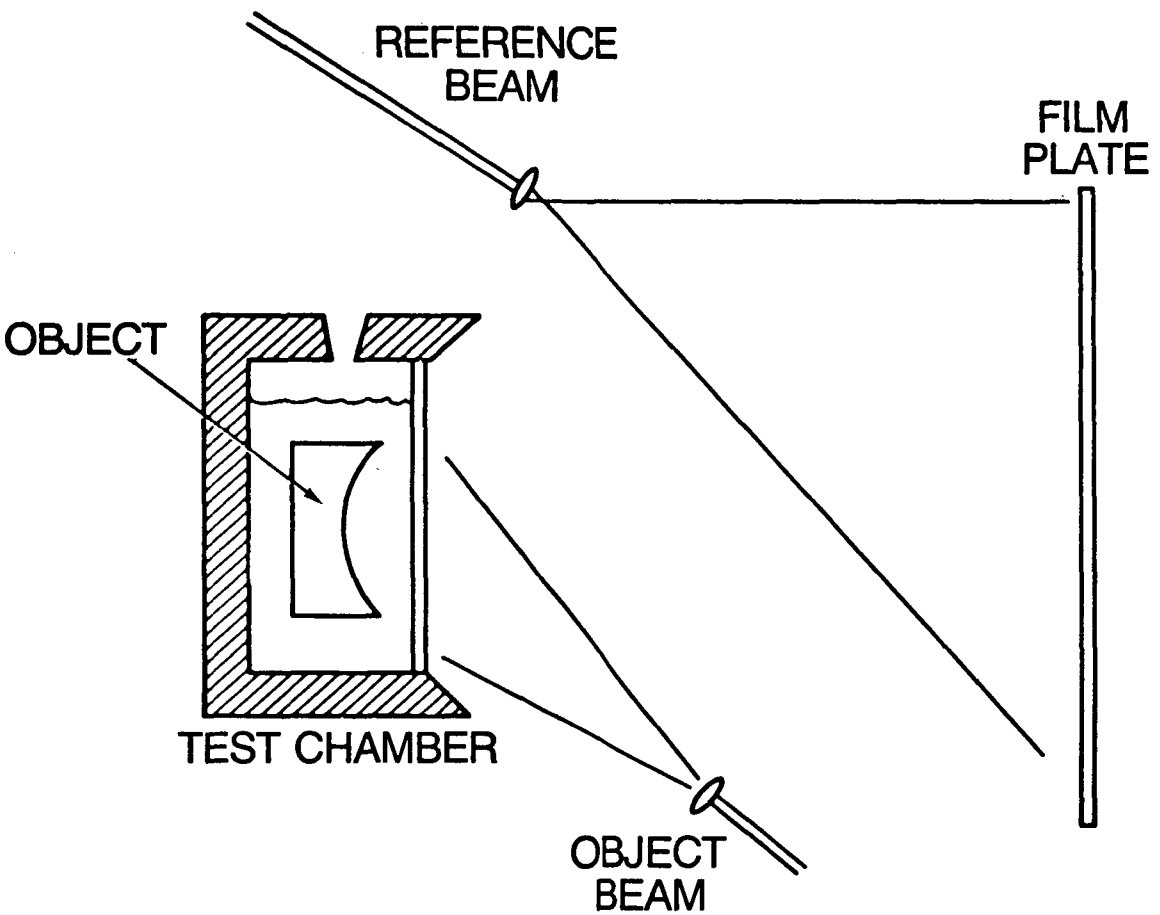

This display and the associated equation are keys to understanding the strength and shortcomings of holographic measurement techniques. The display is traced from an actual holographic contour interferogram. The contour of this object is somewhat like that of a spoon with its deepest point to the right of the picture. To interpret this homodyne interferogram, one could simply count the interference fringes. Obviously the resolution obtained by counting would be rather poor - perhaps half of a fringe, corresponding to an optical path length difference measurement resolution of one quarter of the optical wavelength (about .125 μm).

The actual image intensity as shown in the plot and expressed in the equation to the right is a continuous function of the surface displacement, D. Unfortunately, the intensity pattern is also a function of the average image intensity (without fringes) and the interferometric fringe contrast. Thus the homodyne interferogram intensity at any point may be represented as an equation in three unknowns where the desired variable, D, cannot yet be solved for directly.

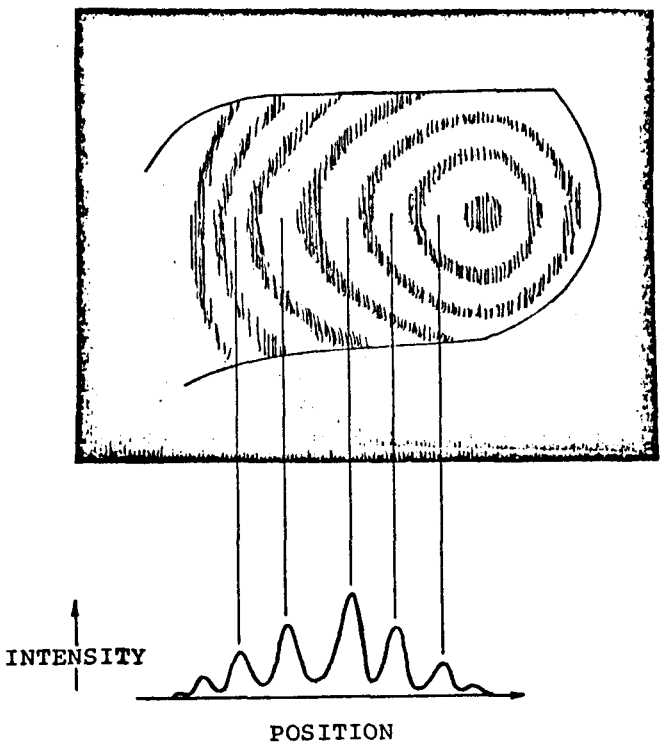

$$I = I_o[1+C \sin(2kD)]$$

I = Measured Intensity

I_o = Image Intensity

C = Fringe Contrast

D = Displacement

Homodyne Display

Q-HHI and HHI offer two means by which one may solve for the variable, D. In order to do so, however, a new optical recording arrangement must be used. In this case, two angularly distinct reference beams are used sequentially in the double-exposure recording process - reference beam #1 for the first exposure then reference beam #2 for the second exposure after the object is stressed. Upon reconstruction reference #1 reconstructs the first object wavefront and reference #2 reconstructs the second.

Heterodyne Recording

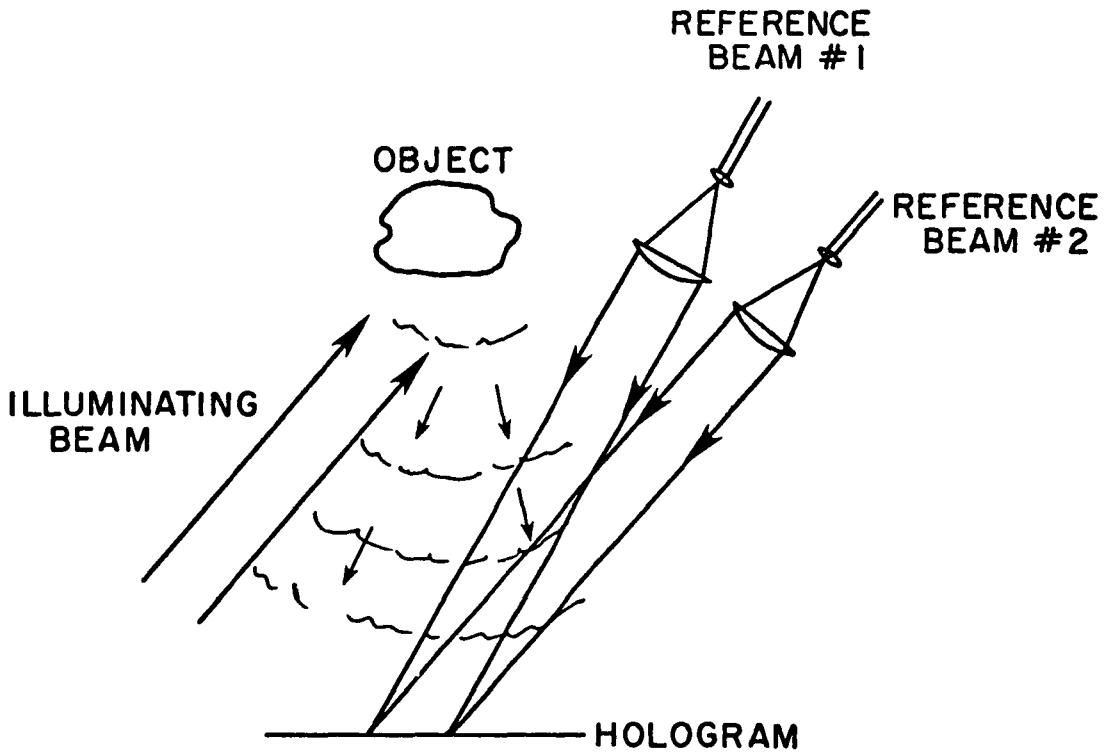

This figure illustrates the recording and playback setup which would be used to perform HHI contouring.

Contouring Using HHI

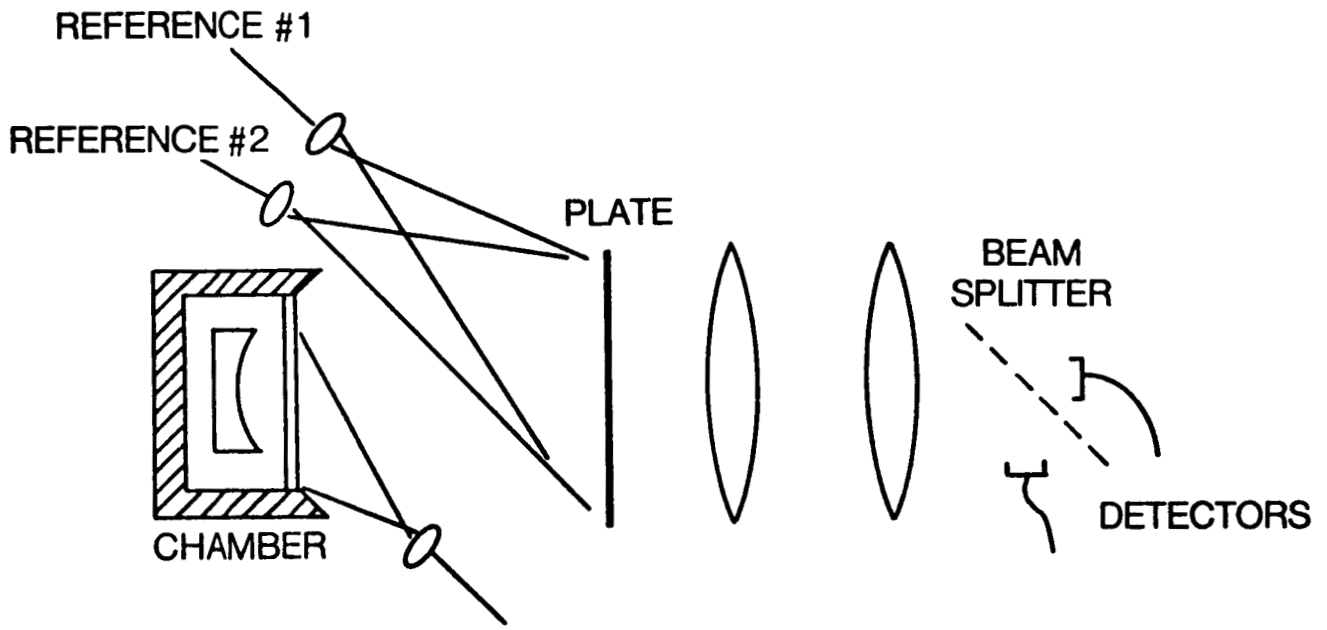

Once exposed and developed, the double exposure, dual reference beam hologram may be analyzed either by the quasi-heterodyne or heterodyne readout process. The Q-HHI process requires a digital image processing system to perform some arithmetic operations on the interference images. A phase shifter (optical delay) is placed in one of the reference beams and is used to shift the position of the fringes.

To perform the analysis, a homodyne image is viewed by the video camera and recorded in the digital image processor. Subsequently, a phase shift is imposed in one reference beam and a second image is recorded. After a second phase shift, a third image is recorded. At any point, the intensity of the image in the three video images may be represented respectively by the three equations shown. Note that these equations are essentially the same as the homodyne equations with the addition of a phase term contributed by the phase shifter. Since these phase terms are known, one is left with a system of three equations in three unknowns which can be solved directly for D.

Quasi-Heterodyne Readout

$$I_1 = I_o[1+C\sin(2kD+\Delta\phi_1)]$$

$$I_2 = I_o[1+C\sin(2kD+\Delta\phi_2)]$$

$$I_3 = I_o[1+C\sin(2kD+\Delta\phi_3)]$$

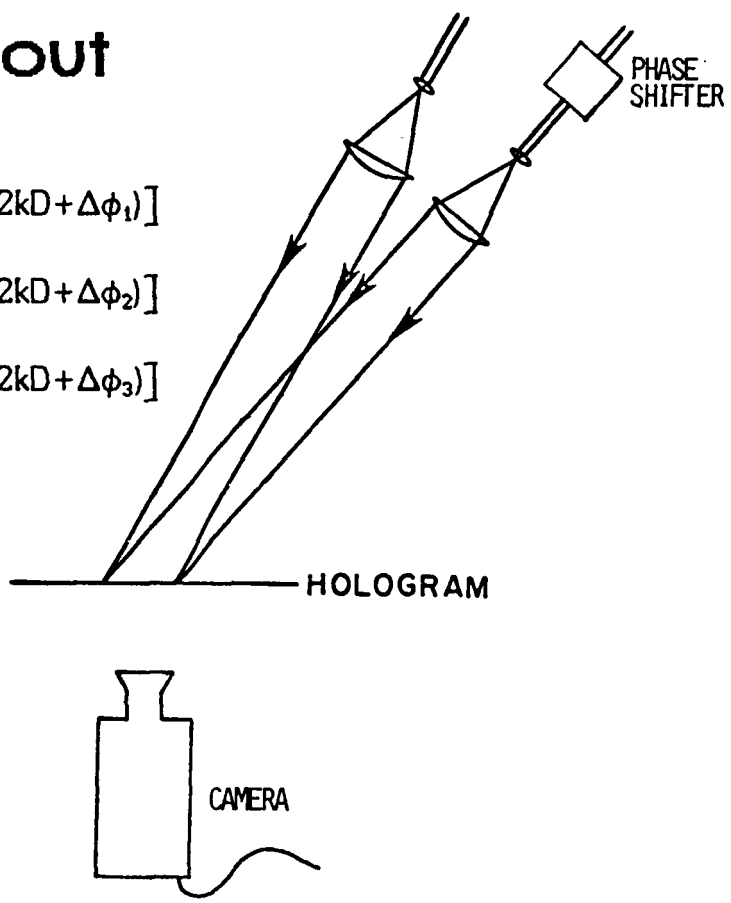

The result of the simultaneous solution involving the three images is itself an image whose pixel intensity is a function of elevation or displacement (left). Alternatively, the data may be displayed in perspective (right).

Wear Contours

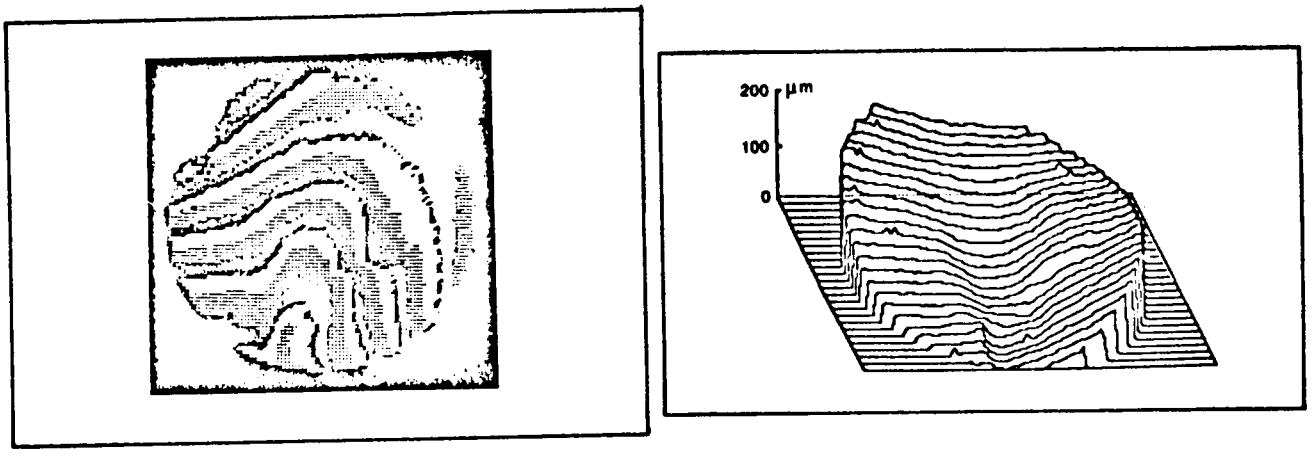

HHI readout requires that a frequency shifter be inserted into one of the reference beams. Typical shift values are 100 kHz and may be obtained with a combination of Bragg cell modulators. The resulting image intensity fluctuates sinusoidally with time at the shift frequency. While all image points vary in intensity at the same frequency, the phase at which the fluctuations take place is a function of local surface displacement or contour (D) as shown in the equation.

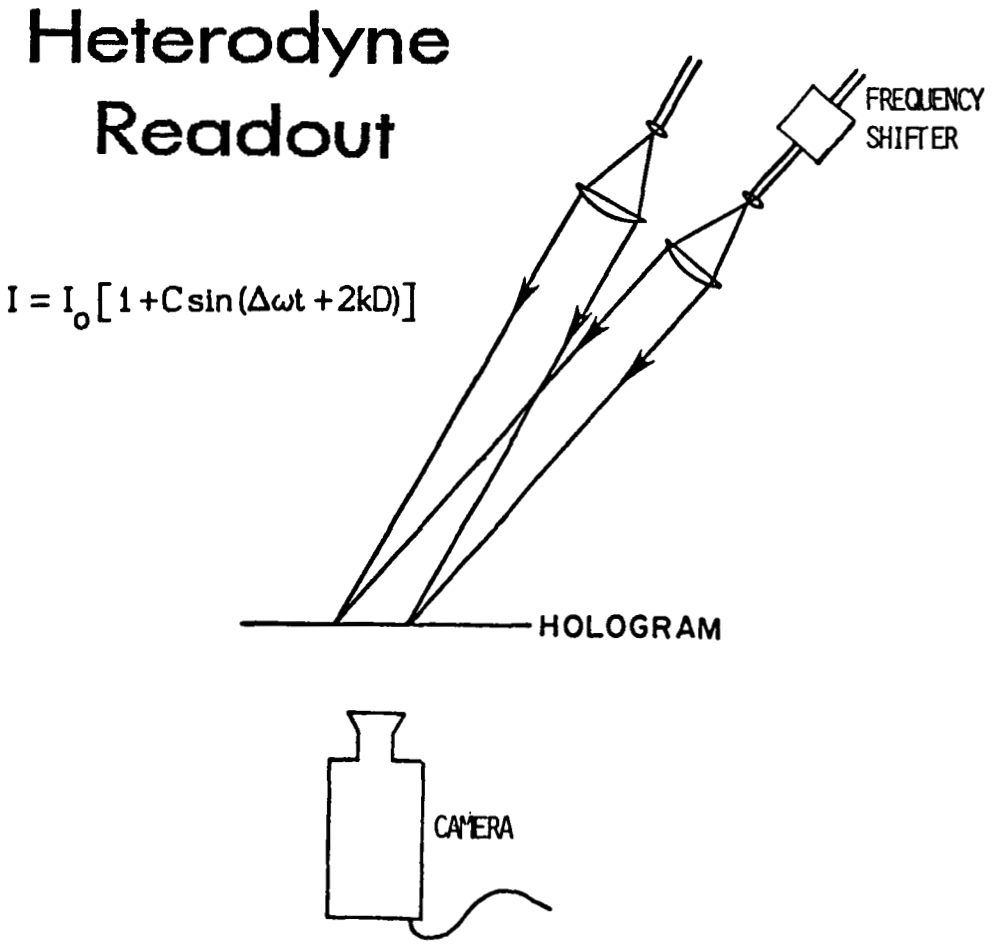

An image dissector camera or a translatable single-point detector is placed in the output plane of the interferometer. By comparing the phase of the intensity fluctuations at each point with the phase at some image reference point, the displacement, D, (or contour) may be directly measured independent of fringe contrast or spatial variations in object intensity. If an electronic phase meter is used whose accuracy is 0.360 degrees, for example, it is clear that one should be able to measure displacements to 1/1000 of a fringe! (At this point one begins to encounter some secondary spatial noise effects which may limit the certainty of such measurements.)

The fringes drawn in this figure are there for reference to the homodyne image. In heterodyning, the fringes "move" at the shift frequency and are not seen.

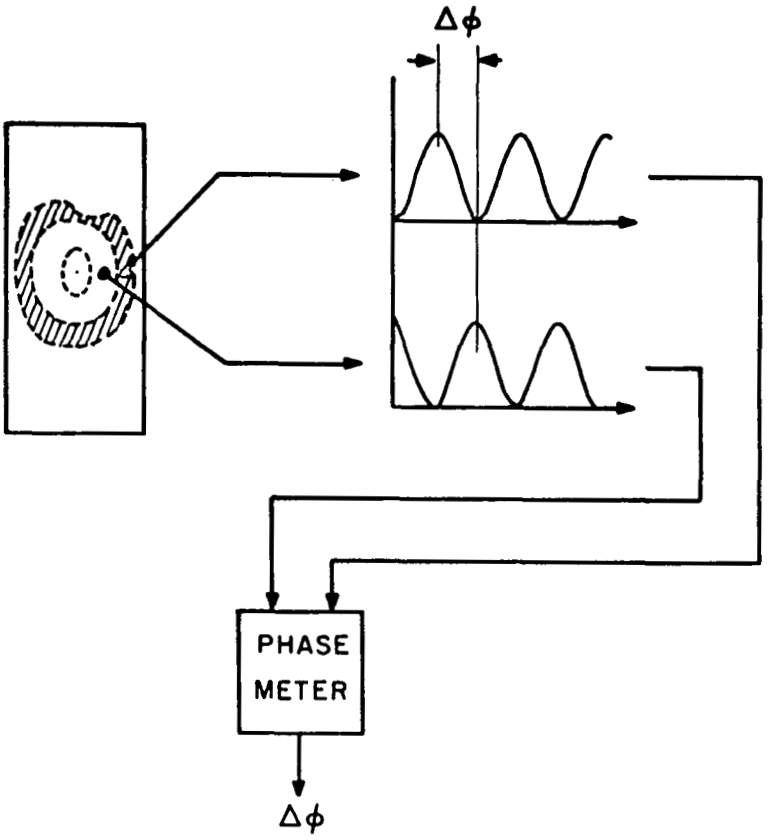

Contour map of a section of the spoon shaped object showing a wear gouge running down the center is shown. Note that the apparently poor resolution is the inability to "desensitize" holographic fringes by the double refractive index contouring technique. The actual optical path length difference resolution obtained during this experiment was about 3 Angstroms.

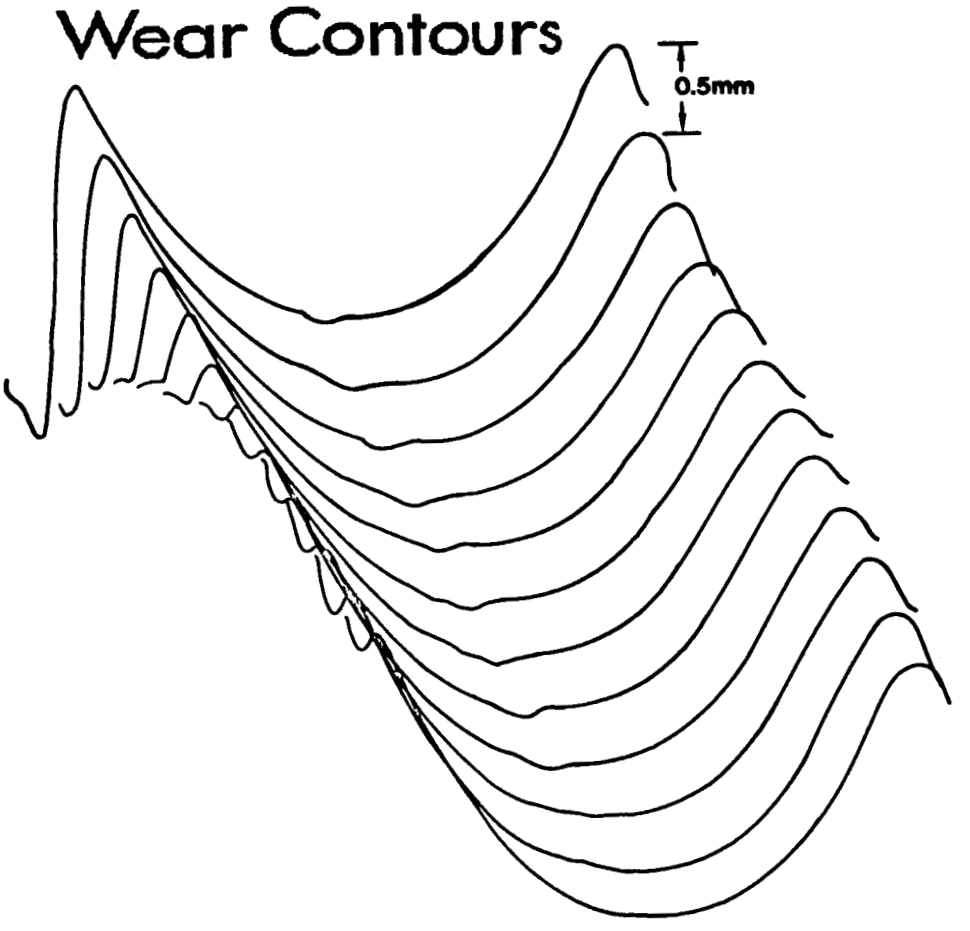

This HHI map of an acoustic surface wave propagating across an aluminum specimen demonstrates the ability to record and analyze high-speed, transient phenomena. The recording time was 9 nanoseconds. OPD resolution was 9 Angstroms.

Surface Acoustic Wavefront

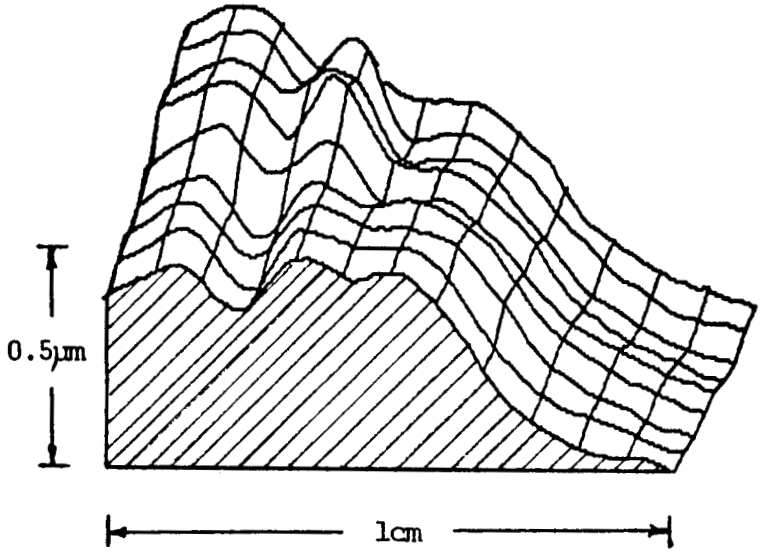

Several advantages are listed. Machine interpretability is unique to Q-HHI and HHI and holds promise for machine vision and intelligent processing (AI).

Advantages

Noncontacting

Very high out-of-plane resolution and dynamic range

Full field measurement and display

Machine interpretable

These limitations represent current state of the art in HHI and are not physical limits. Indeed they represent two of the challenges being addressed by the thrust of our current research activities.

Limitations

Highest resolution requires long analysis time and high readout system stability

Relatively poor (25-100μm) lateral resolution compared with out-of-plane resolution